

GAN-Based Multiple Adjacent Brain MRI Slice Reconstruction for Unsupervised Alzheimer’s Disease Diagnosis

Changhee Han^{1,2,3}(✉), Leonardo Rundo^{4,5}, Kohei Murao²,
Zoltán Ádám Milacski⁶, Kazuki Umemoto⁷, Evis Sala^{4,5},
Hideki Nakayama^{3,8}, and Shin’ichi Satoh²

¹ LPIXEL Inc., Tokyo, Japan
han@lpixel.net,

² Research Center for Medical Big Data,
National Institute of Informatics, Tokyo, Japan

³ Graduate School of Information Science and Technology,
The University of Tokyo, Tokyo, Japan

⁴ Department of Radiology, University of Cambridge, Cambridge, United Kingdom

⁵ Cancer Research UK Cambridge Centre, Cambridge, United Kingdom

⁶ Department of Artificial Intelligence,
ELTE Eötvös Loránd University, Budapest, Hungary

⁷ Department of Rehabilitation Medicine,
Juntendo University School of Medicine, Tokyo, Japan

⁸ International Research Center for Neurointelligence (WPI-IRCIN), The University
of Tokyo Institutes for Advanced Study, The University of Tokyo, Tokyo, Japan

Abstract. Unsupervised learning can discover various diseases, relying on large-scale unannotated medical images of healthy subjects. Towards this, unsupervised methods reconstruct a single medical image to detect outliers either in the learned feature space or from high reconstruction loss. However, without considering continuity between multiple adjacent slices, they cannot directly discriminate diseases composed of the accumulation of subtle anatomical anomalies, such as Alzheimer’s Disease (AD). Moreover, no study has shown how unsupervised anomaly detection is associated with disease stages. Therefore, we propose a two-step method using Generative Adversarial Network-based multiple adjacent brain MRI slice reconstruction to detect AD at various stages: (*Reconstruction*) Wasserstein loss with Gradient Penalty + ℓ_1 loss—trained on 3 healthy slices to reconstruct the next 3 ones—reconstructs unseen healthy/AD cases; (*Diagnosis*) Average/Maximum loss (e.g., ℓ_2 loss) per scan discriminates them, comparing the reconstructed/ground truth images. The results show that we can reliably detect AD at a very early stage with Receiver Operating Characteristics-Area Under the Curve (ROC-AUC) 0.780 while also detecting AD at a late stage much more accurately with ROC-AUC 0.917; since our method is fully unsupervised, it should also discover and alert any anomalies including rare disease.

Keywords: Generative adversarial networks · Alzheimer’s disease diagnosis · Unsupervised anomaly detection · Brain MRI reconstruction.

1 Introduction

Deep Learning can achieve accurate computer-assisted diagnosis when large-scale annotated training samples are available. In medical imaging, unfortunately, preparing such massive annotated datasets is often unfeasible; to tackle this important problem, researchers have proposed various data augmentation techniques, including Generative Adversarial Network (GAN)-based ones [1–5]. However, even exploiting these techniques, supervised learning still requires many images with pathological features, even for rare disease, to make a reliable diagnosis; nevertheless, it can only detect already-learned specific pathologies. In this regard, as physicians notice previously unseen anomaly examples using prior information on healthy body structure, unsupervised anomaly detection methods leveraging only large-scale healthy images can discover and alert the presence of the disease when their generalization fails.

Towards this, researchers reconstructed a single medical image *via* GANs [6], AutoEncoders (AEs) [7], or combining them, since GANs can generate realistic images and AEs, especially Variational AEs, can directly map data onto its latent representation [8]; then, unseen images were scored by comparing them with reconstructed ones to discriminate a pathological image distribution (i.e., outliers either in the learned feature space or from high reconstruction loss). However, those single image reconstruction methods mainly target diseases easy-to-detect from a single image even for non-expert human observers, such as glioblastoma on Magnetic Resonance Imaging (MRI) [8] and lung cancer on Computed Tomography images [7]. Without considering continuity between multiple adjacent images, they cannot directly discriminate diseases composed of the accumulation of subtle anatomical anomalies, such as Alzheimer’s Disease (AD). Moreover, no study has shown so far how unsupervised anomaly detection is associated with disease stages. We thus propose a two-step method using GAN-based multiple adjacent brain MRI slice reconstruction to detect AD at various stages (Fig. 1): (*Reconstruction*) Wasserstein loss with Gradient Penalty (WGAN-GP) [9, 10] + ℓ_1 loss—trained on 3 healthy brain axial MRI slices to reconstruct the next 3 ones—reconstructs unseen healthy/AD cases; (*Diagnosis*) Average/Maximum loss (e.g., ℓ_2 loss) per scan discriminates them, comparing the reconstructed and ground truth images.

Contributions. Our main contributions are as follows:

- **MRI Slice Reconstruction:** This first multiple MRI slice reconstruction approach can predict the next 3 brain MRI slices from the previous 3 ones only for unseen images similar to training data by combining WGAN-GP and ℓ_1 loss.
- **Unsupervised Anomaly Detection:** This first unsupervised anomaly detection across different disease stages reveals that, like physicians’ way of diagnosis, massive healthy data can reliably aid early diagnosis, such as of Mild Cognitive Impairment (MCI), while also detecting late-stage disease much more accurately by discriminating with ℓ_2 loss.

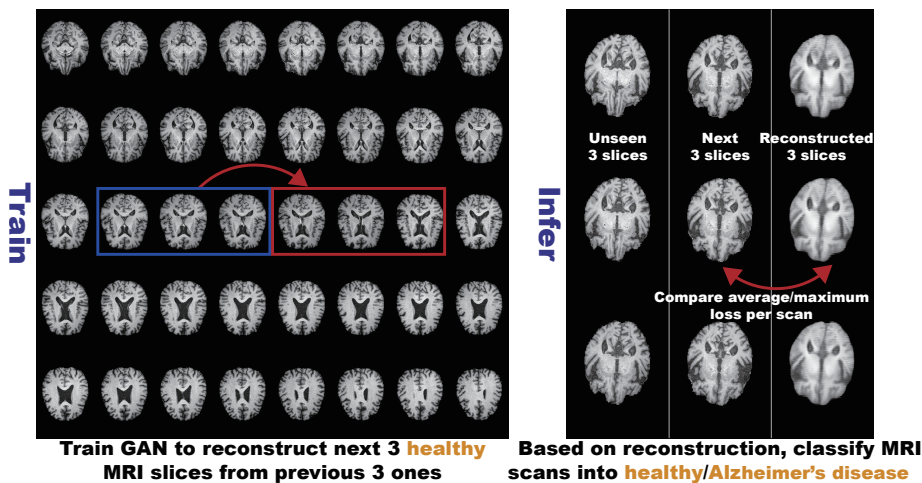


Fig. 1. Unsupervised AD diagnosis framework: we train WGAN-GP + ℓ_1 loss on 3 healthy brain axial MRI slices to reconstruct the next 3 ones, and test it on both unseen healthy and AD cases to classify them based on average/maximum loss (e.g., ℓ_2 loss) per scan.

- **Alzheimer’s Disease Diagnosis:** This first unsupervised AD diagnosis study can reliably detect AD and also other diseases.

The remainder of the manuscript is organized as follows: Sect. 2 outlines the state-of-the-art of automated AD diagnosis; Sect. 3 describes the analyzed MRI dataset, as well as the proposed GAN-based unsupervised AD diagnosis framework; experimental results are shown and discussed in Sect. 4; finally, Sect. 5 provides conclusive remarks and future work.

2 Automated Alzheimer’s Disease Diagnosis

Despite the clinical, social, and economic significance of early AD diagnosis—primarily associated with MCI detection—it generally relies on subjective assessment by physicians (e.g., neurologists, geriatricians, and psychiatrists); to tackle this open challenge, researchers have used classic supervised Machine Learning based on hand-crafted features [11, 12]. More recently, Deep Learning has attracted great attentions owing to its more abstract and descriptive embedding based on multiple non-linear transformations: Liu *et al.* used a semi-supervised CNN to significantly reduce the need for labeled training data [13]; for clinical decision-making, Suk *et al.* integrated multiple sparse regression models (namely, Deep Ensemble Sparse Regression Network) [14]; Spasov *et al.* devised a parameter-efficient CNN for 3D separable convolutions, combining dual learning and a specific layer to predict the conversion from MCI to AD within 3 years [15];

instead of exploiting the CNNs, Parisot used a semi-supervised Graph Convolutional Network trained on a sub-set of labeled nodes with diagnostic outcomes to represent sparse clinical data [16].

To the best of our knowledge, no existing work has conducted fully unsupervised anomaly detection for AD diagnosis since capturing subtle anatomical differences between MCI and AD is challenging. Therefore, without requiring any labeled data for training, the proposed GAN-based unsupervised approach might provide new insights into AD research.

3 Materials and Methods

3.1 OASIS-3 Dataset

We use a longitudinal dataset of $176 \times 240/176 \times 256$ T1-weighted (T1w) 3T brain axial MRI slices containing both normal aging subjects/AD patients extracted from the Open Access Series of Imaging Studies-3 (OASIS-3) [17]. The 176×240 slices are zero-padded to reach 176×256 pixels. Relying on Clinical Dementia Rating (CDR) [18], common clinical scale for the staging of dementia, the subjects are comprised of:

- Unchanged CDR = 0: Cognitively healthy population;
- CDR = 0.5: Very mild dementia (\sim MCI);
- CDR = 1: Mild dementia;
- CDR = 2: Moderate dementia.

Since our dataset is longitudinal and the same subject’s CDRs may vary (e.g., CDR = 0 to CDR = 0.5), we only use scans with unchanged CDR = 0 to assure certainly healthy scans. As CDRs and MRI scans are not always simultaneously acquired, we label MRI scans with CDRs at the closest date. We only select brain MRI slices including hippocampus/amygdala/ventricles among whole 256 axial slices per scan to avoid over-fitting from AD-irrelevant information; the atrophy of the hippocampus/amygdala/cerebral cortex, and enlarged ventricles are strongly associated with AD, and thus they mainly affect the AD classification performance of Machine Learning [19]. Moreover, we discard low-quality MRI slices. The remaining dataset is divided as follows:

- Training set: Unchanged CDR = 0 (408 subjects/1,133 scans/57,834 slices);
- Validation set: Unchanged CDR = 0 (55 subjects/155 scans/8,080 slices),
CDR = 0.5 (53 subjects/85 scans/4,607 slices),
CDR = 1 (29 subjects/45 scans/2,518 slices),
CDR = 2 (2 subjects/4 scans/160 slices);
- Test set: Unchanged CDR = 0 (113 subjects/318 scans/16,198 slices),
CDR = 0.5 (99 subjects/168 scans/9,206 slices),
CDR = 1 (61 subjects/90 scans/5,014 slices),
CDR = 2 (4 subjects/6 scans/340 slices).

The same subject’s scans are included in the same dataset. The datasets are strongly biased towards healthy scans similarly to MRI inspection in the clinical routine. During training for reconstruction, we only use the training set containing healthy slices to conduct unsupervised learning.

3.2 GAN-based Multiple Adjacent Brain MRI Slice Reconstruction

To model the strong consistency of healthy brain anatomy (Fig. 1), in each scan, we reconstruct the next 3 MRI slices from the previous 3 ones using an image-to-image GAN (e.g., if a scan includes 40 slices s_i for $i = 1, \dots, 40$, we reconstruct all possible 35 setups: $(s_i)_{i \in \{1,2,3\}} \mapsto (s_i)_{i \in \{4,5,6\}}$; $(s_i)_{i \in \{2,3,4\}} \mapsto (s_i)_{i \in \{5,6,7\}}$; \dots ; $(s_i)_{i \in \{35,36,37\}} \mapsto (s_i)_{i \in \{38,39,40\}}$). We concatenate adjacent 3 grayscale slices into 3 channels, such as in RGB images. The GAN uses: (i) a U-Net-like [20, 21] generator with 4 convolutional and 4 deconvolutional layers in encoders and decoders, respectively, with skip connections; (ii) a discriminator with 3 decoders. We apply batch normalization to both convolution with Leaky Rectified Linear Unit (ReLU) and deconvolution with ReLU. To confirm how reconstructed images’ realism and anatomical continuity affect anomaly detection, we compare the GAN models with different loss functions, namely: (i) Dice loss (i.e., a plain U-Net without the discriminator); (ii) WGAN-GP loss; (iii) WGAN-GP loss + 100 ℓ_1 loss. Among 8 losses comparing ground truth/reconstruction, average ℓ_2 loss per scan always outperforms the other losses during validation for U-Net and WGAN-GP without/with ℓ_1 loss, and thus we use this loss for testing.

Considering its computational speed, U-Net training lasts for 600,000 steps with a batch size of 64 and both GAN trainings last for 300,000 steps with a batch size of 32. We use 2.0×10^{-4} learning rate for the Adam optimizer [22]. The framework is implemented on Keras with TensorFlow as backend.

3.3 Unsupervised Alzheimer’s Disease Diagnosis

During validation, we compare the following average/maximum losses per scan (i.e., 8 losses) between reconstructed/ground truth 3 slices (Fig. 1): (i) ℓ_1 loss; (ii) ℓ_2 loss; (iii) Dice loss; (iv) Structural Similarity loss. For each model’s testing, we separately pick the loss showing the highest Receiver Operating Characteristics-Area Under the Curve (ROC-AUC) between CDR = 0 (i.e., healthy population) *vs* all the other CDRs (i.e., dementia) during validation. As a result, we pick the average ℓ_2 loss per scan for all models since squared error is sensitive to outliers and it always outperforms the others. To evaluate its unsupervised AD diagnosis performance for test sets, we show ROC and Precision-Recall (PR) curves, along with their AUCs, between CDR = 0 *vs* (i) all the other CDRs; (ii) CDR = 0.5; (iii) CDR = 1; (iv) CDR = 2. We visualize ℓ_2 loss distributions of CDR = 0/0.5/1/2 to know how disease stages affect its discrimination.

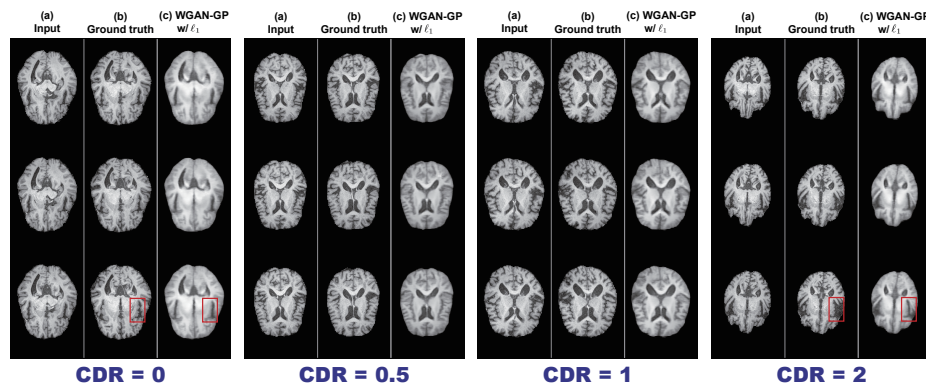


Fig. 2. Example brain MRI slices with $\text{CDR} = 0/0.5/1/2$ from test sets: (a) Input 3 real slices; (b) Ground truth next 3 real slices; (c) Next 3 slices reconstructed by U-Net; (d), (e) Next 3 slices reconstructed by WGAN-GP without/with ℓ_1 loss.

4 Results

4.1 Reconstructed Brain MRI Slices

Fig. 2 illustrates example real MRI slices from test sets and their reconstruction by U-Net and WGAN-GP without/with ℓ_1 loss. The WGAN-GP + ℓ_1 loss can successfully capture T1w-specific appearance and anatomical changes from the previous 3 slices more smoothly than the U-Net and in more detail than the WGAN-GP without ℓ_1 loss. Since the models are trained only on healthy slices, reconstructing slices with higher CDRs tends to comparatively fail, especially around hippocampus, amygdala, cerebral cortex, and ventricles due to their insufficient atrophy after reconstruction.

4.2 Unsupervised AD Diagnosis Results

Figs. 3 and 4 show ROC and PR curves, respectively—along with their AUCs—of unsupervised anomaly detection. We do not show confidence intervals since the diagnosis stage is non-trainable. Since brains with higher CDRs accompany stronger anatomical atrophy from healthy brains, their ROC-AUCs between unchanged $\text{CDR} = 0$ remarkably increase as CDRs increase. Clearly outperforming the other methods in every condition, WGAN-GP + ℓ_1 loss achieves excellent ROC-AUCs, especially for higher CDRs—it obtains ROC-AUC = 0.780/0.833/0.917 for $\text{CDR} = 0$ vs $\text{CDR} = 0.5/1/2$, respectively; this experimental finding derives from ℓ_1 loss’ good realism sacrificing diversity (i.e., generalizing well only for unseen images with a similar distribution to training images) and WGAN-GP loss’ ability to capture recognizable structure. Fig. 5 indicates its good discrimination ability even between healthy subjects vs MCI patients (i.e., $\text{CDR} = 0$ vs $\text{CDR} = 0.5$), which is extremely difficult even in a

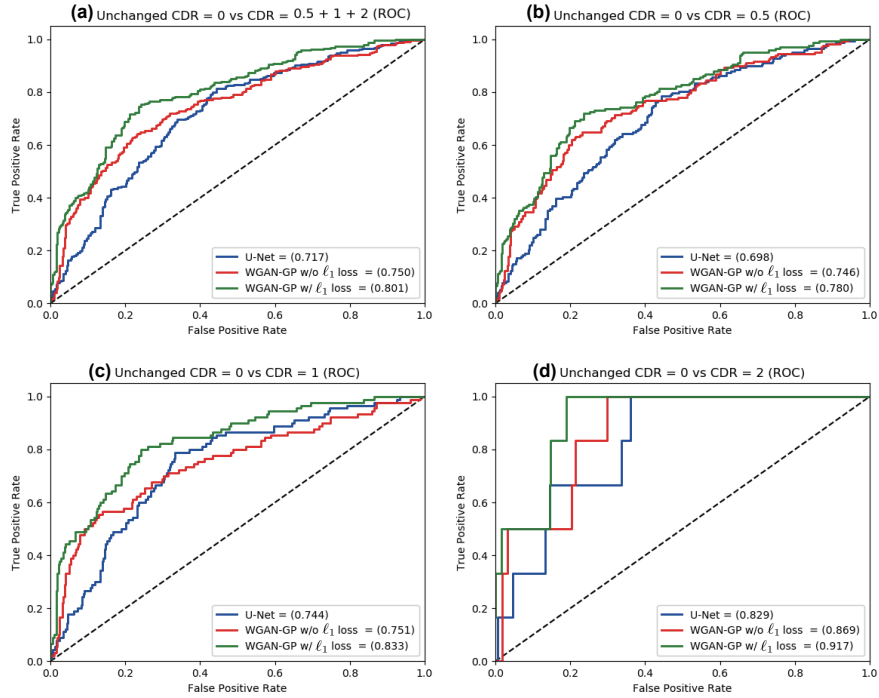


Fig. 3. Unsupervised anomaly detection results using average ℓ_2 loss per scan on reconstructed brain MRI slices (ROC curves and ROC-AUCs): unchanged CDR = 0 (i.e., cognitively healthy population) is compared with (a) all the other CDRs (i.e., dementia); (b) CDR = 0.5 (i.e., very mild dementia); (c) CDR = 1 (i.e., mild dementia); (d) CDR = 2 (i.e., moderate dementia).

supervised manner [19]. Interestingly, unlike our visual expectation, WGAN-GP without ℓ_1 loss outperforms plain U-Net regardless of its very blurred reconstruction, showing the superiority of GAN-based reconstruction for diagnosis.

5 Conclusions and Future Work

Using a massive amount of healthy images, our GAN-based multiple MRI slice reconstruction can successfully discriminate AD patients from healthy subjects for the first time in an unsupervised manner; our solution leverages a two-step approach: (*Reconstruction*) ℓ_1 loss generalizes well only for unseen images with a similar distribution to training images while WGAN-GP loss captures recognizable structure; (*Diagnosis*) ℓ_2 loss clearly discriminates healthy/abnormal data as squared error becomes huge for outliers. Using 1,133 healthy MRI scans for training, our approach can reliably detect AD at a very early stage, MCI, with ROC-AUC = 0.780 while detecting AD at a late stage much more accurately with ROC-AUC = 0.917—implying its ability to detect various other diseases.

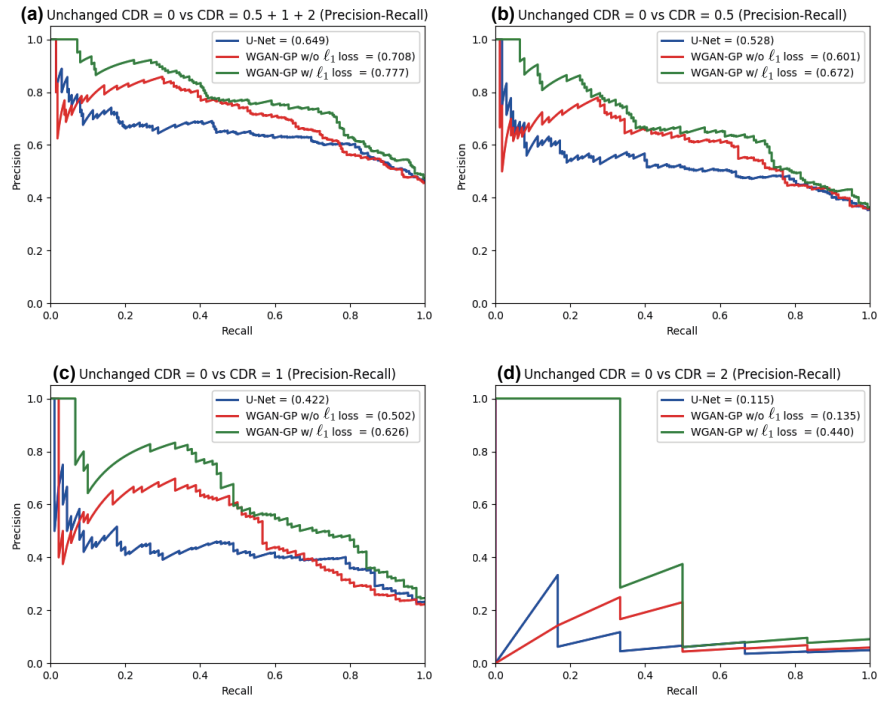


Fig. 4. Unsupervised anomaly detection results using average ℓ_2 loss per scan on reconstructed brain MRI slices (PR curves and PR-AUCs): unchanged CDR = 0 is compared with (a) all the other CDRs; (b) CDR = 0.5; (c) CDR = 1; (d) CDR = 2.

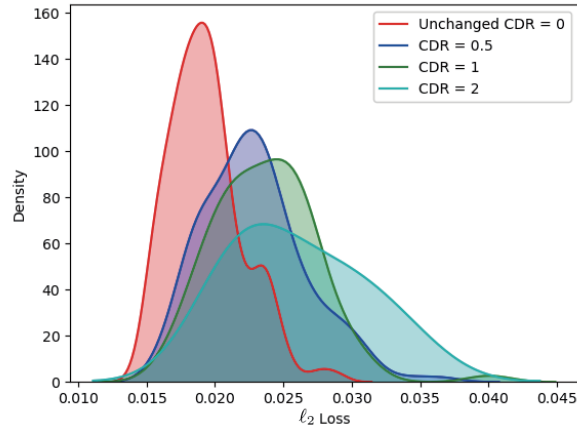


Fig. 5. Distributions of average ℓ_2 loss per scan evaluated on brain MRI slices with CDR = 0/0.5/1/2 reconstructed by WGAN-GP + ℓ_1 loss.

Accordingly, this first unsupervised anomaly detection across different disease stages reveals that, like physicians’ way of diagnosis, large-scale healthy data can reliably aid early diagnosis, such as of MCI, while also detecting late-stage disease much more accurately. Since our method deals well with diseases that are hard-to-detect even in supervised learning, this unsupervised approach should also discover/alert any anomalies including rare disease, where supervised learning is inapplicable [23]. As future work, we will reconstruct slices from both previous/next 3 slices (e.g., slices s_i for $i = 1, \dots, 9$, $(s_i)_{i \in \{1,2,3,7,8,9\}} \mapsto (s_i)_{i \in \{4,5,6\}}$) for robustness, also optimizing the number of slices (e.g., 3 slices to 1 or 5 slices). We will investigate more reconstruction networks (e.g., GANs with attention mechanisms) and multiple loss functions for both reconstruction/diagnosis. Lastly, we plan to detect and locate various diseases, including cancer [24] and rare diseases—this work only uses brain MRI slices including hippocampus/amygdala/ventricles for AD diagnosis, but we may have to use all or most brain MRI slices to also detect anomalies appearing in other anatomical locations within the brain. Integrating multimodal imaging data, such as Positron Emission Tomography with specific radiotracers [25], might further improve AD diagnosis [26], even when analyzed modalities are partially unavailable [27].

Acknowledgment

This research was partially supported by AMED Grant Number JP18lk1010028, and also partially supported by The Mark Foundation for Cancer Research and Cancer Research UK Cambridge Centre [C9685/A25177]. Additional support has been provided by the National Institute of Health Research (NIHR) Cambridge Biomedical Research Centre. Zoltán Ádám Milacski was supported by Grant Number VEKOP-2.2.1-16-2017-00006. The OASIS-3 dataset has Grant Numbers P50 AG05681, P01 AG03991, R01 AG021910, P50 MH071616, U24 RR021382, and R01 MH56584.

References

1. Goodfellow, I., Pouget-Abadie, J., Mirza, M., Xu, B., Warde-Farley, D., Ozair, S., et al.: Generative adversarial nets. In: Proceedings of Advances in Neural Information Processing Systems (NIPS). (2014) 2672–2680
2. Frid-Adar, M., Diamant, I., Klang, E., Amitai, M., Goldberger, J., Greenspan, H.: GAN-based synthetic medical image augmentation for increased CNN performance in liver lesion classification. *Neurocomputing* **321** (2018) 321–331
3. Han, C., Rundo, L., Araki, R., Nagano, Y., Furukawa, Y., et al.: Combining noise-to-image and image-to-image GANs: brain MR image augmentation for tumor detection. *IEEE Access* **7**(1) (2019) 156966–156977
4. Han, C., Kitamura, Y., Kudo, A., Ichinose, A., Rundo, L., Furukawa, Y., et al.: Synthesizing diverse lung nodules wherever massively: 3D multi-conditional GAN-based CT image augmentation for object detection. In: Proc. International Conference on 3D Vision (3DV). (2019) 729–737

5. Han, C., Murao, K., Noguchi, T., et al.: Learning more with less: Conditional PGGAN-based data augmentation for brain metastases detection using highly-rough annotation on MR images. In: Proc. ACM International Conference on Information and Knowledge Management (CIKM). (2019) 119–127
6. Schlegl, T., Seeböck, P., Waldstein, S.M., Langs, G., Schmidt-Erfurth, U.: f-AnoGAN: fast unsupervised anomaly detection with generative adversarial networks. *Med. Image Anal.* **54** (2019) 30–44
7. Uzunova, H., Schultz, S., Handels, H., Ehrhardt, J.: Unsupervised pathology detection in medical images using conditional variational autoencoders. *Int. J. Comput. Assist. Radiol. Surg.* **14**(3) (2019) 451–461
8. Chen, X., Konukoglu, E.: Unsupervised detection of lesions in brain MRI using constrained adversarial auto-encoders. In: International Conference on Medical Imaging with Deep Learning (MIDL). (2018) arXiv preprint arXiv:1806.04972.
9. Gulrajani, I., Ahmed, F., Arjovsky, M., Dumoulin, V., Courville, A.C.: Improved training of Wasserstein GANs. In: Advances in Neural Information Processing Systems. (2017) 5769–5779
10. Han, C., Hayashi, H., Rundo, L., Araki, R., Shimoda, W., Muramatsu, S., et al.: GAN-based synthetic brain MR image generation. In: Proc. International Symposium on Biomedical Imaging (ISBI), IEEE (2018) 734–738
11. Salvatore, C., Cerasa, A., Battista, P., Gilardi, M.C., Quattrone, A., Castiglioni, I.: Magnetic resonance imaging biomarkers for the early diagnosis of Alzheimer’s disease: a machine learning approach. *Front. Neurosci.* **9** (2015) 307
12. Nanni, L., Brahnay, S., Salvatore, C., Castiglioni, I.: Texture descriptors and voxels for the early diagnosis of Alzheimer’s disease. *Artif. Intell. Med.* **97** (2019) 19–26
13. Liu, S., Liu, S., Cai, W., Pujol, S., Kikinis, R., Feng, D.: Early diagnosis of alzheimer’s disease with deep learning. In: Proc. International Symposium on Biomedical Imaging (ISBI), IEEE (2014) 1015–1018
14. Suk, H.I., Lee, S.W., Shen, D.: Deep ensemble learning of sparse regression models for brain disease diagnosis. *Med. Image Anal.* **37** (2017) 101–113
15. Spasov, S., Passamonti, L., Duggento, A., Liò, P., Toschi, N., Initiative, A.D.N., et al.: A parameter-efficient deep learning approach to predict conversion from mild cognitive impairment to Alzheimer’s disease. *NeuroImage* **189** (2019) 276–287
16. Parisot, S., Ktena, S.I., Ferrante, E., Lee, M., Guerrero, R., Glocker, B., Rueckert, D.: Disease prediction using graph convolutional networks: application to autism spectrum disorder and Alzheimer’s disease. *Med. Image Anal.* **48** (2018) 117–130
17. LaMontagne, P.J., Keefe, S., Lauren, W., et al.: OASIS-3: longitudinal neuroimaging, clinical, and cognitive dataset for normal aging and Alzheimer’s disease. *Alzheimers Dement.* **14**(7) (2018) P1097
18. Morris, J.C.: The Clinical Dementia Rating (CDR): current version and scoring rules. *Neurology* **43**(11) (1993) 2412–2414
19. Ledig, C., Schuh, A., Guerrero, R., Heckemann, R.A., Rueckert, D.: Structural brain imaging in Alzheimer’s disease and mild cognitive impairment: biomarker analysis and shared morphometry database. *Sci. Rep.* **8** (2018) 11258
20. Ronneberger, O., Fischer, P., Brox, T.: U-Net: Convolutional networks for biomedical image segmentation. In: Medical Image Computing and Computer-Assisted Intervention (MICCAI). Volume 9351 of LNCS., Springer (2015) 234–241
21. Rundo, L., Han, C., Nagano, Y., et al.: USE-Net: incorporating squeeze-and-excitation blocks into U-Net for prostate zonal segmentation of multi-institutional MRI datasets. *Neurocomputing* **365** (2019) 31–43

22. Kingma, D.P., Ba, J.: Adam: A method for stochastic optimization. arXiv preprint arXiv:1412.6980 (2014)
23. Han, C., Rundo, L., Murao, K., Nemoto, T., Nakayama, H., Satoh, S.: Bridging the gap between AI and healthcare sides: towards developing clinically relevant AI-powered diagnosis systems. In: Proc. International Conference on Artificial Intelligence Applications and Innovations (AIAI). (2020)
24. Rundo, L., Militello, C., Russo, G., Vitabile, S., Gilardi, M.C., Mauri, G.: GTVcut for neuro-radiosurgery treatment planning: an MRI brain cancer seeded image segmentation method based on a cellular automata model. *Nat. Comput.* **17** (2018) 521–536
25. Rundo, L., Stefano, A., Militello, C., Russo, G., Sabini, M.G., D'Arrigo, C., Marletta, F., Ippolito, M., Mauri, G., Vitabile, S., Gilardi, M.C.: A fully automatic approach for multimodal PET and MR image segmentation in Gamma Knife treatment planning. *Comput. Methods Programs Biomed.* **144** (2017) 77–96
26. Brier, M.R., Gordon, B., Friedrichsen, K., McCarthy, J., Stern, A., Christensen, J., Owen, C., Aldea, P., Su, Y., Hassenstab, J., et al.: Tau and $A\beta$ imaging, CSF measures, and cognition in Alzheimer's disease. *Sci. Trans. Med.* **8**(338) (2016) 338ra66–338ra66
27. Li, R., Zhang, W., Suk, H.I., Wang, L., Li, J., Shen, D., Ji, S.: Deep learning based imaging data completion for improved brain disease diagnosis. In: Medical Image Computing and Computer-Assisted Intervention (MICCAI). Volume 8675 of LNCS., Springer (2014) 305–312